

Negative dysphotopsia: The enigmatic penumbra

Jack T. Holladay, MD, MSEE, Huawei Zhao, PhD, Carina R. Reisin, PhD

PURPOSE: To determine the cause of negative dysphotopsia and the location, appearance, and relative intensity of such images in pseudophakic eyes.

SETTING: Baylor College of Medicine, Houston, Texas, USA.

DESIGN: Reporting available data addressing a specific clinical question.

METHODS: Negative dysphotopsia was simulated using the Zemax optical design program. The nominal values for the pseudophakic eye model were as follows: IOL power, 20.0 diopters (D); corneal power, 43.5 D; Q value, -0.26 ; axial IOL depth behind pupil, 0.5 mm; external anterior chamber depth (corneal vertex to iris plane), 4.0 mm; optic diameter, 6.0 mm; pupil diameter, 2.5 mm.

RESULTS: From the first ray-tracing simulation, analysis of the image for the nominal parameters showed 2 annuli (ring-shaped) shadows. The inner annulus shadow was located from a retinal visual field angle of 86.0 to 100.0 degrees (width 14.0 degrees), and the outer annular shadow was located from 105.9 to 123.3 degrees (width 17.4 degrees). Superimposing the inner annulus on the human visual field showed that the shadow would be apparent only temporally, where it is within the limits of the visual field and functional retina. The patient would perceive this as a temporal dark crescent-shaped partial shadow (penumbra).

CONCLUSIONS: Primary optical factors required for negative dysphotopsia are a small pupil, a distance behind the pupil of 0.06 mm or more and 1.23 mm or less for acrylic, a sharp-edged design, and functional nasal retina that extends anterior to the shadow. Secondary factors include a high index of refraction optic material, angle α , and the nasal location of the pupil relative to the eye's optical axis.

Financial Disclosure: Drs. Zhao and Reisin are employees of and Dr. Holladay is a consultant to Abbott Medical Optics, Inc. No author has a financial or proprietary interest in any material or method mentioned.

J Cataract Refract Surg 2012; 38:1251–1265 © 2012 ASCRS and ESCRS

Unwanted optical images can arise after the implantation of intraocular lenses (IOLs). These include dysphotopsia, defined as unwanted patterns on the retina that can be positive or negative. Positive dysphotopsia consists of bright artifacts, such as arcs,¹ streaks,² rings, or halos³ on the retina centrally or midperipherally, but not on the extreme periphery. Negative dysphotopsia is the absence of light reaching certain portions of the retina that manifests as a dark shadow.

Negative dysphotopsia, first described more than 10 years ago,⁴ manifests as a temporal dark crescent-shaped shadow after in-the-bag posterior chamber IOL implantation. The mechanism of this disorder has remained a clinical enigma, with proposed explanations that include IOL material with a high index of refraction,^{4–6} optics with a sharp or truncated edge,^{4,6} idiosyncratic predisposition,⁷ a cataract incision

located temporally in clear cornea,⁸ brown irides,⁸ a prominent globe,⁹ a shallow orbit,⁹ an IOL anterior surface that is more than 0.46 mm from the plane of the posterior iris,⁹ a negative afterimage,¹⁰ neural adaptation,¹⁰ and reflection of the anterior capsulotomy edge projected onto the nasal peripheral retina.¹¹ Several additional articles and letters with case reports showing the absence of some of these suggested mechanisms have also been published.^{12–15} Some of these clinical observations may be valid and were summarized by Masket and Fram¹¹ in their 10 clinical manifestations.

In 1999, Holladay et al.,¹ using a nonsequential ray-tracing technique, compared the image and relative intensity of reflected glare images from 4 commonly used IOL edge designs to assess the potential for noticeable postoperative edge glare. Their results indicated that a sharp or truncated optic edge was

the most significant factor in positive dysphotopsia due to an intense peak of reflected glare light on the retina. A few years later, Erie et al.^{16,17} found that reflections from the front and back surfaces of equiconvex unequal biconvex designs and a higher index of refraction optic materials were also factors that increased the relative intensity of the reflected light from 300- to 3500-fold above that of the crystalline lens. Several subsequent studies¹⁸⁻³² confirmed these factors to be important in producing positive dysphotopsia.

The phenomenon of negative dysphotopsia has remained an enigma. To date there has been little theoretical exploration and computer modeling to explain negative dysphotopsia. The current study was designed to evaluate negative dysphotopsia using ray tracing and to illustrate the phenomenon using a common light source (direct ophthalmoscope) and lens in an effort to explain relevant observations and to review methods of eliminating the problem from clinical practice.

MATERIALS AND METHODS

Eye-Model Specifications

The Zemax optical design program (Zemax Development Corp.) was used to evaluate negative dysphotopsia. The program generates ray-tracing models of simple and complex optical systems based on user-defined specifications. Figure 1 shows the nominal values used in this study's pseudophakic model. Other values for these parameters were also used to determine their effect on the image location as follows: IOL power, 10.0 D and 30.0 D; corneal power, 40.5 D and 46.5 D; axial IOL depth behind pupil, 0.0 mm and 1.0 mm; external ACD, 3.5 mm and 4.5 mm; and pupil diameter, 5.0 mm.

The extended light source (object) was Ganzfeld (similar to a Goldmann or Humphrey visual field perimeter), which extended from 0 degree (foveal fixation) to 125 degrees peripherally (along the visual axis of the eye model) and 360 degrees around the visual axis 1 m from the nodal point of the eye model, which was located near the posterior vertex

of the IOL. The IOL edge design was sharp, truncated, or round (Figure 2).

Ray-Tracing Calculations

Two types of ray-tracing calculations were performed. In the first ray-tracing simulation, the extended light source (Ganzfeld) was treated as a Lambertian scattering object. (Each point on the surface was treated as a point source.) It would be identical to the Goldmann visual field perimeter as the object, except it is at 1 m (rather than 33 cm). The analyses traced 1 billion rays from the extended source through the pupil in the pseudophakic eye model, with the large number of rays ensuring an adequate intensity and spatial location on the retina for each possible condition above. The intensity and the location of all light rays reaching the simulated pseudophakic eye model retina were recorded as shown for the 2.5 mm pupil in Figure 3.

In the second ray-tracing simulation, only the horizontal section was considered. Because the ray tracing is radially symmetric around the optical axis, this provides a conceptual model that can be used to envision the optical performance of the IOL in a single plane. Rays from 0 to 125 degrees were traced to determine the minimum and maximum angles in which a ray could pass through the pupil and edge of the IOL for the nominal and other values shown in Table 1. The coordinates of the intercepts at each surface and the location of all light rays reaching the simulated pseudophakic eye model retina are recorded in Table 1 and shown in Figure 4 for the nominal parameters and a 2.5 mm pupil.

Finally, a direct ophthalmoscope was used as an extended light source to project a beam of light onto and near the edge of a 20.0 D IOL, as shown in the upper part of the 3 images in Figure 5.

RESULTS

From the first ray-tracing simulation using a Lambertian light source, analysis of the image of the extended light source using the nominal parameters for a 2.5 mm pupil specified in Table 1 showed 2 annular (ring-shaped) shadows (Figure 3). The inner annulus shadow was located from a retinal field angle of 86.0 to 100.0 degrees (width 14.0 degrees), and the outer annular shadow was located from 105.9 to 123.3 degrees (17.4 degrees wide). Table 1 shows the ray-tracing values for the nominal values and all other combinations of variables. The 4 primary factors determining the presence and location of a shadow were the size of the pupil, the axial distance of the IOL behind the iris, a sharp or truncated edge, and the high index of refraction optic material (acrylic).

Table 1 shows that the lower index of refraction silicone compared with acrylic moved the anterior border of the shadow forward by approximately 5 degrees and the posterior border forward by 15 degrees, reducing the width of the shadow from 14.0 degrees for acrylic to 2.3 degrees for silicone. The exact width and location of the shadows were not appreciably affected by the dioptric power of the IOL, external ACD, or power of the cornea. As the pupil size was

Submitted: February 11, 2011.

Final revision submitted: January 27, 2012.

Accepted: January 29, 2012.

From the Department of Ophthalmology (Holladay), Baylor College of Medicine, Houston, Texas, and Abbott Medical Optics (Zhao, Reisin), Santa Ana, California, USA.

Presented in part at the annual meeting of the Association for Research in Vision and Ophthalmology, Fort Lauderdale, Florida, USA, April 2008.

Corresponding author: Jack T. Holladay, MD, MSEE, Holladay Consulting, Inc., PO Box 717, Bellaire, Texas 77402-0717, USA. E-mail: holladay@docholladay.com.

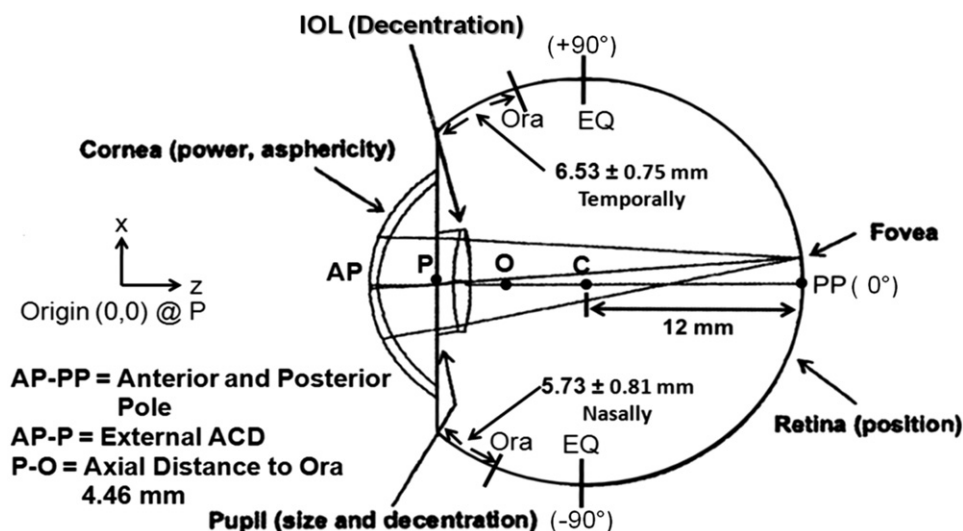


Figure 1. Horizontal section of the schematic human right pseudophakic eye used for Zemax modeling. The pseudophakic eye model had the following nominal values: IOL power = 20.0 D; corneal power = 43.5 D; Q-value = -0.26; axial IOL depth from corneal epithelial vertex to anterior vertex of IOL = 4.0 mm; external ACD from corneal epithelial vertex to iris plane = 4.0 mm; IOL optic diameter = 6 mm; index of refraction of IOL optic material (acrylic) = 1.550; pupil diameter = 2.5 mm; retinal radius = 12.0 mm (center @ "C"). The origin (0,0) for the x-axis and z-axis is P, the center of the pupil. The retinal field angle is 0 degrees at the posterior pole (PP), +90 degrees and -90 degrees at the temporal and nasal equatorial retina, respectively. The edge design of the IOL was sharp or truncated or partially rounded, as shown in Figure 2 (ACD = anterior chamber depth; EQ = equator; IOL = intraocular lens).

increased to 5.0 mm, the location of the shadow remained the same, but the edges became indistinct and rays from other angles fell into the shadow, reducing its contrast so it would not be visible to an observer (Figure 6). Figure 7 is the ray tracing for the horizontal section for Figure 6 using the 5.0 mm pupil.

Superimposing the image (annular shadow) for the 2.5 mm pupil and nominal values with the sharp-edged optic on the human visual field showed that only the temporal portion of the inner annular shadow would be apparent, where it is within the limits of the visual field and functional retina (Figure 8). The patient would perceive a temporal dark crescent-shaped

shadow through a 2.5 mm pupil (Figures 3 and 4) and no shadow through a 5.0 mm pupil (Figures 6 and 7).

Using a direct ophthalmoscope as an extended light source and a 20.0 D IOL, a shadow was illustrated when the light source was incident on the edge of the IOL such that unrefracted light rays passed by and refracted light passed through the edge of the IOL (Figure 5).

DISCUSSION

Unwanted shadows in most optical systems are a result of discontinuities in the system where 2 adjacent

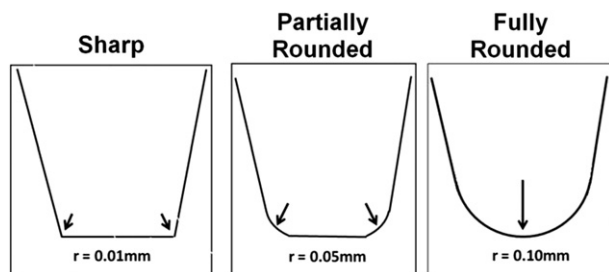


Figure 2. Sharp-edged and round-edged optics. A sharp or truncated edge will have sharp corners anteriorly and posteriorly as opposed to the rounded corners (middle and right panels). Sharp to rounded edges are a spectrum for which the exact radius is specific to the manufacturer. A partially rounded edge with a radius of 0.05 mm would still have approximately 50% of the edge flat, while a fully rounded edge with a 0.10 mm radius would fully round an edge with a 0.20 mm edge thickness. In this study's model, the nominal value of 0.05 mm was used for the corner radii of the rounded edge. The fully rounded edge was not used because the partially rounded was sufficient to disperse the rays and avoid a shadow (r = radius).

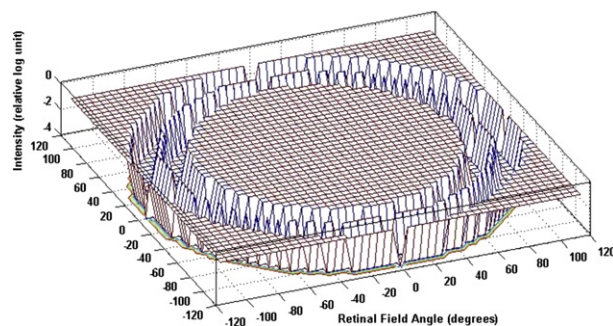


Figure 3. Ray tracing in the model of the acrylic sharp-edged optic (while using the nominal parameters with a 2.5 mm pupil diameter, 0.5 mm behind the iris, and the Ganzfeld object) showed 2 ring-shaped shadows that were located using retinal field angles (retinal intercepts in Table 1) from 86.0 to 100.0 degrees (14.0 degrees wide) and from 105.9 to 123.3 degrees (17.4 degrees wide). The relative intensity of the shadows (10^{-4}) were approximately $1000\times$ less than the lighted surrounding area (10^{-1}) on the retina and would appear black to an observer. There was no visible shadow using the round-edged optic (Figure 6).

Table 1. Ray Tracing Intercepts in Figure 12 (Sharp/Truncated Edge Optic) for Nominal* and Additional Parameters with the Origin of the Coordinates at the Pupillary Center (Figure 1).

Origin Ray Description	Variable Changed from Nominal	Initial Angle Theta(°)	Ray 1 Cornea Intercept			Pupil Plane Intercept			Ray 2 Ant IOL Intercept			Ray 3 Edge IOL Intercept			Ray 4 Post IOL Intercept			Ray 1 Retinal Intercept		Posterior Border of Shadow: Ray 3 Retinal Intercept		Anterior Border of Shadow: Ray 4 Retinal Intercept		Retinal Field Angle Omega(°)				
			z (mm)	x (mm)	Theta(°)	z (mm)	x (mm)	Theta(°)	z (mm)	x (mm)	Theta(°)	z (mm)	x (mm)	Theta(°)	z (mm)	x (mm)	Theta(°)	z (mm)	x (mm)	z (mm)	x (mm)	z (mm)	x (mm)					
Vertex of IOL 0.0 mm Posterior to Pupillary Plane																												
Max Angle [‡]	Nominal*	NONE	No limiting pupillary rays could pass through point "P" or "A" with the anterior vertex of the IOL at the pupillary plane for Nominal or any Additional Parameters																									
Min Angle [‡]	Nominal	NONE																										
Max Angle	Additional	NONE																										
Min Angle	Additional	NONE																										
Vertex of IOL 0.5 mm Posterior to Pupillary Plane																												
Max Angle	Nominal	93.4	-0.802	6.377	-81.2	0.0	1.220	-81.3	0.645	-2.980	-51.3	0.661	-3.000	-44.3				1.723	-10.03	9.180	-11.948				-86.0			
Min Angle	Nominal	81.0	-2.372	4.763	-68.5	0.0	-1.250	-66.9	0.621	-2.705	-50.7				0.856	-2.992	-58.6							6.254	-11.825	-100.0		
Max Angle	K=40.5	94.6	-0.832	6.597	-81.2	0.0	1.234	-81.3	0.647	-2.996	-53.1	0.650	-3.000	-46.4				1.713	-10.03	9.175	-11.952				6.400	-11.848	-99.3	
Min Angle	K=40.5	81.1	-2.508	4.727	-67.2	0.0	-1.250	-67.1	0.621	-2.721	-49.9				0.855	-2.999	-57.9								6.400	-11.848	-99.3	
Max Angle	K=46.5	92.4	-0.601	5.810	-82.5	0.0	1.250	-81.3	0.647	-2.994	-56.3	0.651	-3.000	-46.4				1.714	-10.03	9.180	-11.949					6.418	-11.852	-86.0
Min Angle	K=46.5	79.0	-2.464	4.493	-66.8	0.0	-1.250	-67.0	0.620	-2.711	-50.0				0.856	-2.992	-57.9								6.418	-11.852	-99.2	
Max Angle	ACD=3.5	95.4	-0.768	5.983	-80.8	0.0	1.250	-81.3	0.642	-2.940	-55.0	0.684	-3.000	-46.2				1.689	-9.669	9.219	-11.909					6.021	-11.667	-85.8
Min Angle	ACD=3.5	84.4	-2.077	4.477	-70.1	0.0	-1.250	-66.9	0.621	-2.706	-51.2				0.855	-2.997	-59.2								6.021	-11.667	-101.2	
Max Angle	ACD=4.5	89.1	-1.271	6.417	-78.4	0.0	0.216	-78.6	0.647	-2.990	-55.0	0.654	-3.000	-45.9				2.187	-10.6	9.274	-11.904						-85.6	
Min Angle	ACD=4.5	78.0	-2.653	5.044	-67.1	0.0	-1.250	-67.0	0.620	-2.710	-50.0				0.856	-2.991	-58.0								6.446	-11.921	-99.1	
Max Angle	IOL=30	93.4	-0.802	6.377	-81.2	0.0	1.220	-81.3	0.645	-2.980	-51.3	0.661	-3.000	-44.3				1.723	-10.03	9.180	-11.948						-86.0	
Min Angle	IOL=30	81.0	-2.378	4.753	-68.4	0.0	-1.250	-67.3	0.623	-2.741	-50.4				0.834	-2.996	-56.1								6.815	-11.903	-97.3	
Max Angle	IOL=10	93.5	-0.786	6.403	-81.3	0.0	1.240	-81.3	0.645	-2.980	-49.6	0.662	-3.000	-44.3				1.723	-10.03	9.180	-11.948						-86.0	
Min Angle	IOL=10	81.0	-2.353	4.789	-68.7	0.0	-1.250	-66.8	0.618	-2.690	-50.5				0.868	-2.993	-62.2								5.430	-11.653	-104.0	
Max Angle	Dec. Pupil [§]	92.9	-0.875	6.332	-80.8	0.0	0.940	-80.7	0.647	-2.995	-51.3	0.651	-3.000	-44.3				1.797	-10.08	9.200	-11.944						-85.9	
Min Angle	Dec. Pupil	75.3	-2.901	3.969	-62.3	0.0	-1.550	-62.4	0.623	-2.740	-47.8				0.855	-2.996	-54.9								7.147	-11.940	-95.7	
Max Angle	n=1.460 [¶]	91.5	-0.955	6.265	-79.22	0.0	1.250	-79.9	0.753	-2.980	-59.0	0.765	-3.000	-44.3				2.071	-10.26	7.620	-11.964						-93.5	
Min Angle	n=1.460	76.0	-2.731	4.226	-63.49	0.0	-1.250	-63.5	0.697	-2.649	-51.8				0.961	-2.985	-55.41								7.134	-11.938	-95.8	
Vertex of IOL 1.0 mm Posterior to Pupillary Plane																												
Max Angle	Nominal	85.6	-1.100	5.276	-74.7	0.0	1.250	-74.9	1.147	-2.993	-54.5	1.152	-3.000	-44.3				3.286	-10.89	10.207	-11.846						-81.1	
Min Angle	Nominal	65.2	-3.287	3.228	-53.7	0.0	-1.250	-53.8	1.127	-2.788	-42.4				1.355	-2.996	-48.0								9.403	-11.935	-84.9	
Max Angle	K=40.5	86.7	-1.340	6.123	-74.6	0.0	1.250	-74.9	1.147	-2.995	-51.3	1.151	-3.000	-44.4				3.277	-10.89	10.199	-11.846						-81.1	
Min Angle	K=40.5	66.0	-3.304	3.286	-53.9	0.0	-1.250	-53.8	1.128	-2.790	-42.4				1.355	-2.997	-48.0								9.396	-11.937	-85.0	
Max Angle	K=46.5	83.9	-1.314	5.747	-73.7	0.0	1.250	-74.7	1.138	-2.916	-52.7	1.202	-3.000	-45.0				3.425	-10.96	10.025	-11.838						-81.9	
Min Angle	K=46.5	64.4	-3.286	3.133	-53.1	0.0	-1.250	-53.7	1.127	-2.785	-42.2				1.356	-2.993	-47.9								9.430	-11.935	-84.8	
Max Angle	ACD=3.5	87.5	-1.161	5.599	-75.1	0.0	1.250	-74.9	1.146	-2.988	-50.2	1.156	-3.000	-44.4				3.209	-10.61	10.259	-11.902						-80.8	
Min Angle	ACD=3.5	67.1	-2.966	2.811	-53.9	0.0	-1.250	-53.3	1.125	-2.757	-42.5				1.36	-2.972	-48.2								9.405	-11.963	-84.9	
Max Angle	ACD=4.5	84.1	-1.382	6.326	-74.8	0.0	1.245	-74.9	1.147	-2.996	-53.1	1.150	-3.000	-44.9				3.345	-11.14	9.988	-11.794						-82.1	
Min Angle	ACD=4.5	63.9	-3.578	3.651	-53.9	0.0	-1.250	-53.8	1.127	-2.788	-42.1				1.355	-2.994	-48.3								9.299	-11.900	-85.4	
Max Angle	IOL=30	85.6	-1.100	5.276	-74.7	0.0	1.250	-74.9	1.147	-2.993	-54.5	1.152	-3.000	-44.3				3.286	-10.89	10.207	-11.846						-81.1	
Min Angle	IOL=30	66.0	-3.259	3.288	-54.3	0.0	-1.250	-54.1	1.129	-2.808	-42.4				1.335	-2.996	-46.7								9.737	-11.910	-83.3	
Max Angle	IOL=10	85.6	-1.100	5.276	-74.7	0.0	1.250	-74.9	1.147	-2.993	-54.5	1.152	-3.000	-44.3				3.286	-10.89	10.207	-11.846						-81.1	
Min Angle	IOL=10	64.9	-3.300	3.120	-52.9	0.0	-1.250	-53.5	1.126	-2.771	-42.4				1.367	-2.991	-50.1								8.864	-11.967	-87.5	
Max Angle	Dec. Pupil [§]	84.6	-1.438	5.825	-73.6	0.0	0.94	-73.7	1.146	-2.988	-50.2	1.156	-3	-44.3				7.645	-10.97	10.17	-11.829						-81.3	
Min Angle	Dec. Pupil	59.9	-3.587	2.473	-48.3	0.0	-1.55	-48.2	1.13	-2.814	-38.7				1.355	-2.994	-43.5								10.605	-11.77	-79.1	
Max Angle	n=1.460 [¶]	84.0	-1.401	5.861	-73.1	0.0	1.250	-73.5	1.255	-2.993	-60.3	1.259	-3.000	-51.5				3.645	-11.06	8.406	-11.990						-89.7	
Min Angle	n=1.460	62.4	-3.397	2.978	-51.2	0.0	-1.250	-51.1	1.216	-2.759	-43.5				1.459	-2.99	-46.0								10.034	-11.869	-81.9	

*Nominal Values: K=43.5 D, Q=-0.26, ACD=4.0 mm, Pupil Diameter=2.5mm, Total IOL Power=20D, Front Surface Power =7D, Posterior Surface Power =13D, IOL Diameter =6.0mm, Center Thickness =0.63mm, Edge Thickness =0.2mm, IOL Index of Refraction =1.550

[‡]Maximum temporal limiting pupillary ray through point "P" — Posterior Border of Shadow

[§]Minimum temporal limiting pupillary ray through point "A" — Anterior Border of Shadow

[¶]Pupil decentered nasally by 2.6° (0.3 mm @ cornea plane) to average human physiologic location

^{¶¶}Optic material changed to silicone with Index of Refraction = 1.460

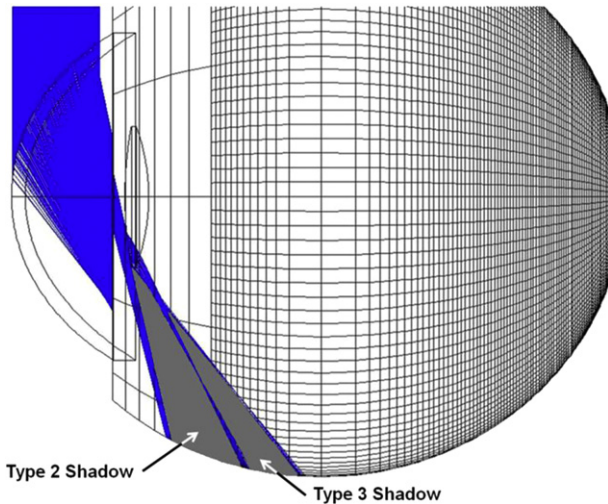


Figure 4. Horizontal ray tracing using nominal values of schematic right eye and a 2.5 mm pupil with the IOL optic 0.5 mm behind the iris. The type 2 shadow is bounded anteriorly by the unrefracted ray, just missing the IOL, and posteriorly by the refracted ray passing through the anterior then posterior surfaces. The type 3 shadow is bounded anteriorly by the ray passing through the anterior then posterior surfaces near the nasal edge and posteriorly by the ray passing through anterior surface then the anterior edge of the IOL. Figure 12 shows a magnified detail of the rays passing through the IOL for the type 3 shadow.

incident rays follow entirely different paths. In cameras, telescopes, and binoculars, these discontinuities are avoided by the inclusion of field stops (apertures) that prevent rays of light from missing the first or all refractive surfaces. In the human eye, the field stop is the pupil, which drapes over the anterior surface of the crystalline lens and prevents rays from passing through the pupil without striking the anterior surface of the crystalline lens. Also, the crystalline lens has a smooth, fully rounded edge (not sharp or truncated), which also prevents discontinuities.

At least 3 optical possibilities would explain a shadow in the extreme temporal field from

discontinuities introduced by a posterior chamber IOL. They are the total internal reflection from rays exceeding the critical angle, an anterior sharp edge, and a posterior sharp edge.

Type 1 Shadow: Internal Reflection

Regarding the type 1 shadow, internal reflection, we previously described how the internal reflection of rays exceeding the critical angle creates positive dysphotopsia.¹ A glare source located approximately 35 degrees off the visual axis was found to create an internal reflection within the IOL that projects onto the temporal retina (Figure 9). The discontinuity is the critical angle of the IOL material surrounded by aqueous ($n = 1.336$) that causes a ray to totally reflect internally rather than refract when it exceeds this angle (Figure 9). For acrylic ($n = 1.55$), poly(methyl methacrylate) ($n = 1.49$), and silicone ($n = 1.46$) in aqueous, the critical angles are 59.5 degrees, 63.7 degrees, and 66.2 degrees, respectively. The critical angle for acrylic is 6.7 degrees less than for silicone, resulting in a greater chance for internal reflection (rays from 59.5 to 90.0 degrees for acrylic versus 66.2 to 90.0 degrees for silicone).

Erie et al.^{16,17} showed that these reflections from IOLs could have a 1090- to 6000-fold brighter relative intensity than those from the unaccommodated human crystalline lens due to reflections from the front and back surface of the equiconvex and asymmetric biconvex IOLs of varying materials. The conditions to produce positive dysphotopsia from the edge would also require the pupil to be large enough for the incident ray to strike near the edge of the IOL, as occurs in low mesopic or scotopic conditions. The internally reflected rays cause positive dysphotopsia on the temporal retina and create a variable intensity image (partial shadows) or streaky vision on the nasal retina as a result of the missing rays.

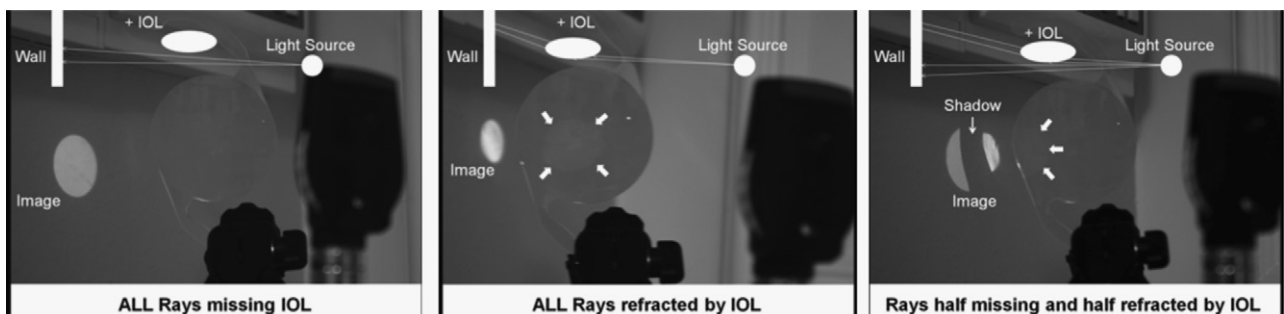


Figure 5. Using a direct ophthalmoscope as an extended light source and a 20.0 D IOL, a shadow develops when refracted and unrefracted light rays pass through the edge of the IOL. Any IOL with positive dioptric power (convergent) would create this shadow due to the way the IOL causes the rays to deviate, as shown in the upper part of the illustration on the right. This second type of shadow appears regardless of the edge design. The arrows indicate the edges of the beam of light striking the IOL. It appears as a faint circle or part of a circle (IOL = intraocular lens).

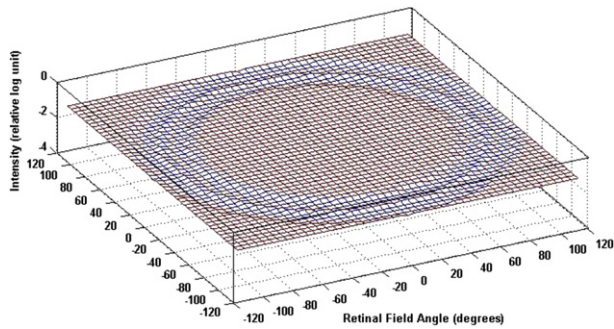


Figure 6. Ray tracing in the model for the sharp-edged optic (using the nominal parameters with a 5.0 mm pupil diameter, the IOL optic 0.5 mm behind the iris, and the Ganzfeld object) showed 2 ring-shaped shadows (highlighted in blue). However, the relative intensity of the shadows was not significantly different from the lighted surrounding area (10^{-1}) on the retina and would not be apparent to an observer. These shadows were located at the same retinal field angles as the 2.5 mm pupil diameter in Figure 3, and the horizontal ray tracing is shown in Figure 7. Again, there was no shadow with the 5.0 mm pupil using the partially round-edged optic.

Under scotopic conditions, the shadow would not be visible because of the dark background (similar to cupping the hand and covering the temporal field).⁸ This area of abnormal vision may sometimes be seen on visual fields (Figure 10) due to the low mesopic testing conditions, as shown by Osher⁸ and described by the patient as a “streaky area” of vision. The relative scotoma is near 35 degrees; however, it would only be noticeable when the pupil is large and the temporal background dimly illuminated, as it is during normal

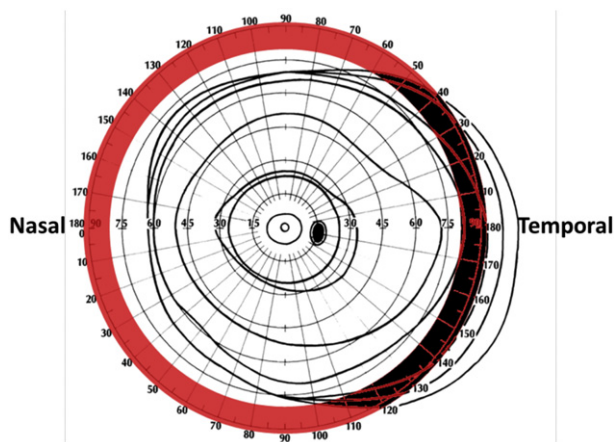


Figure 8. The most peripheral isopter (limit of visual field) is with a 160 mm white test object 1 meter from the patient. Superimposing the image (shadow) in Figure 3 on the human visual field reveals that only the inner shadow would be apparent temporally, where it is within the limits of the visual field (functional retina). The patient would perceive this image as a dark crescent-shaped shadow in the temporal field from 86.0 to 100.0 degrees (14.0 degrees wide, type 3 shadow in Figure 4) to approximately 55 degrees above and approximately 70 degrees below the horizontal.

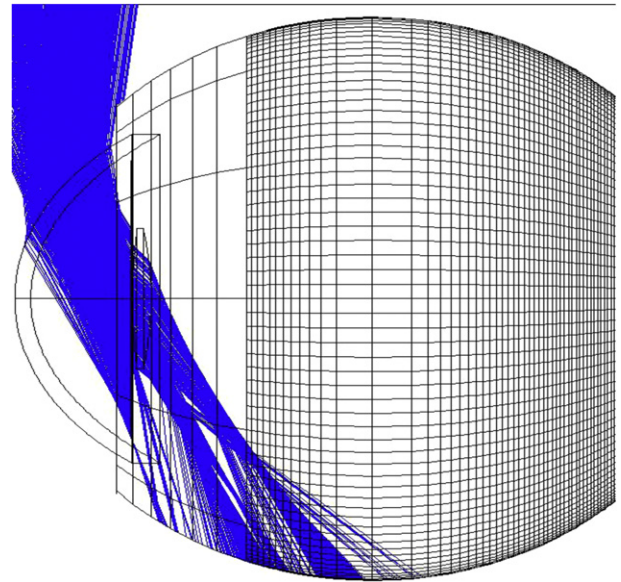


Figure 7. Horizontal ray tracing using nominal values of schematic eye, IOL optic 0.5 mm behind the iris (same parameters as Figure 4) but with a 5.0 mm pupil. There is no demonstrable shadow because the rays all blend together. No shadows would be perceived. Figure 12 shows a magnified detail of the rays passing through the IOL.

visual field testing. Under normal photopic or high mesopic conditions, the pupil is generally too small to allow a ray from 35 degrees to strike the nasal edge of the IOL and cause a shadow.

The case report by Marques and Marques³³ is another good example of a type 1 shadow. The patient reported a dark shadow in the superotemporal field of

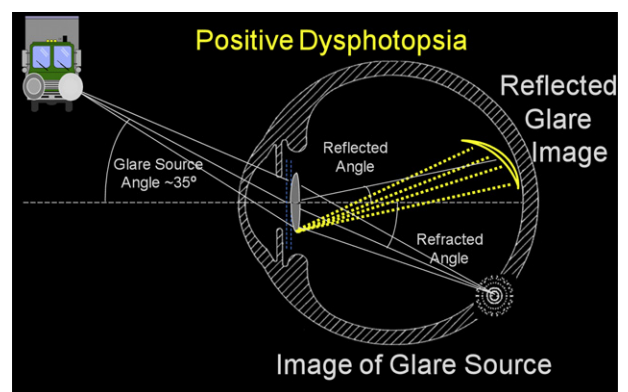


Figure 9. The rays that form the positive dysphotopsia on the temporal retina (reflected glare image) from the square or truncated edge optic would be absent from the refracted image of the light source (image of glare source). The missing rays would cause a variation in the intensity of the image, which would be described as abnormal. In Osher’s patient,⁸ this was described as a “streaky area” on the visual fields (Figure 10) and centered near 35 degrees radially.

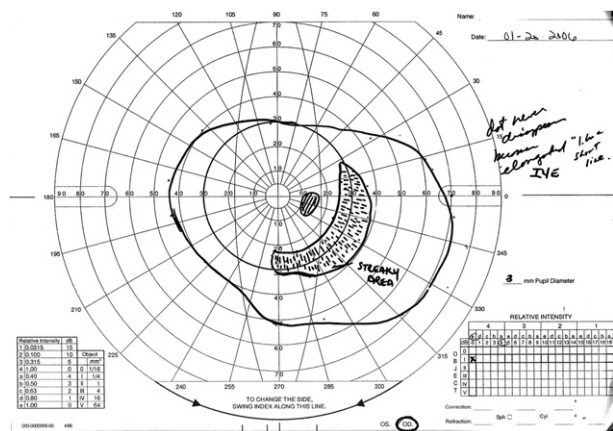


Figure 10. Positive dysphotopsia seen by patient in the nasal field (Figure 9) would create a relative scotoma near 35 degrees in the temporal field due to the missing rays on the nasal retina from internal reflection. Because other rays from the source passing through the posterior surface of the IOL would not be internally reflected, the vision would be described as abnormal, wavy, or a “streaky area” as shown above by Osher.⁸ (Reprinted with permission of the Journal of Cataract & Refractive Surgery. Copyright 2005 American Society of Cataract and Refractive Surgery).

the left eye after implantation of a sharp, truncated in-the-bag posterior chamber IOL. The visual field defect extended irregularly from 10 to 24 degrees temporally and superotemporally, the extent of the Humphrey visual field analyzer using the 24-2 option. The defect is almost identical to that shown with Goldmann visual fields⁸ in Figure 10, except the latter extends to 40 degrees, illustrating the complete area of the defect because the Goldmann tests to 90 degrees (not just 24 degrees). That it disappears with pupil constriction is one of the characteristics of the type 1 shadow and is explained above. The opacification (translucency/diffusivity) of the anterior nasal capsule overlapping the nasal edge of the IOL observed with the biomicroscope is the explanation of the spontaneous resolution of the symptoms by the sixth month, as explained below in the discussion of the natural course and treatments.

This type 1 shadow is not what has been described over the past 10 years as negative dysphotopsia because it disappears with pupil constriction, is near 35 degrees in the visual field (not near 90 degrees), and causes a relative scotoma described as a streaky area rather than an absolute scotoma in the extreme periphery.

Type 2 Shadow: Anterior Sharp IOL Edge Discontinuity

The type 2 shadow results from an anterior sharp IOL edge discontinuity, as shown in Figure 11. Two adjacent rays originating from near 90 degrees temporally are refracted by the midperipheral cornea (by

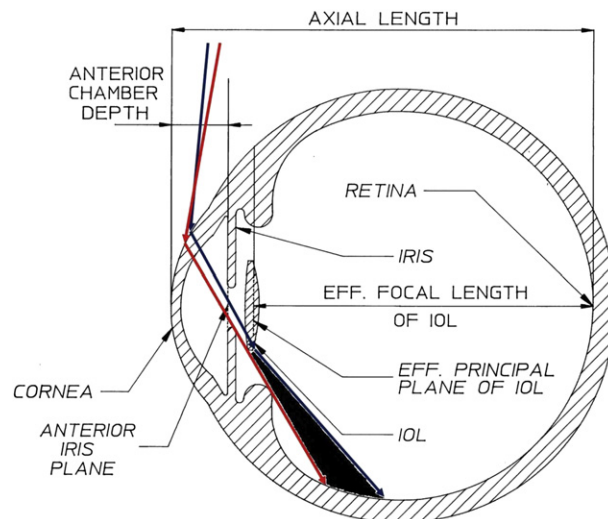


Figure 11. Horizontal section of eye. The red ray just misses the IOL and is not refracted, while the blue ray is refracted by the anterior surface and then the posterior surface of the IOL. The dark region would appear as a shadow if it fell on functional retina (type 2 shadow in Figure 4) (Eff. = effective; IOL = intraocular lens).

~10 degrees to 17 degrees in Table 1, Ray 1 angle theta) and directed toward the pupil. This deviation by the cornea is why the maximum optical visual field angle temporally is approximately 100 to 107 degrees. Any originating ray that is greater than this angle would simply traverse the anterior chamber and could not enter the pupil.

In Figure 11, the red ray just misses the IOL and is not refracted, while the blue ray strikes the front surface of the IOL and is refracted again by the edge or the posterior surface of the IOL near the edge. Then, both are incident on the inner surface of the eye. All positive-power IOLs create this type of shadow because a positive IOL always deviates (converges) an incident ray, whereas the “grazing” ray that misses the IOL is not deviated. The shadow is formed by the angle between these 2 rays. The width of the shadow is almost entirely determined by the optical design of the IOL, specifically the (1) dioptric power, (2) edge design, (3) material, and (4) shape (surface powers). Rounding the front edge of the IOL (Figure 12, right), rather than making it sharp or truncated, disperses rays and prevents formation of a sharply defined shadow.¹

The location of the shadow relative to the beginning of functional retina determines whether the patient perceives negative dysphotopsia. Moses³⁴ has shown that “the retina is not sensitive to light in its periphery, particularly on the temporal side where there are several millimeters of histologically normal retina posterior to the ora that are not represented in the visual field.” Shadows are only perceived if they fall on

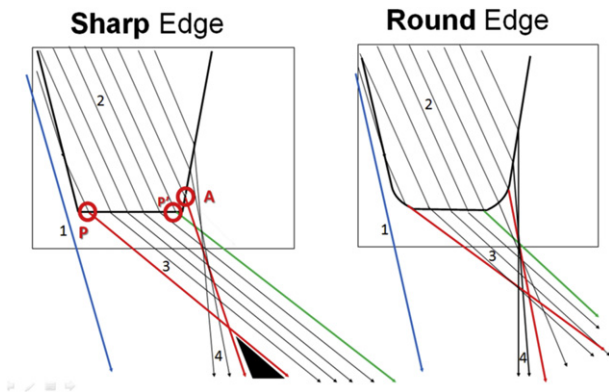


Figure 12. Ray tracing of sharp-edged and round-edged optics. A sharp or truncated edge will have sharp corners anteriorly and posteriorly versus the partially rounded edge corners. (See Figure 2 for radii details.) On the posterior corner of the sharp edge, rays that pass through the edge (3) are refracted more posteriorly than rays passing through the posterior surface (4). For the sharp edge, a shadow (type 3) is present between red rays 3 and 4. The red ray 3 passing through point "P" determines the posterior boundary and the red ray 4 passing through point "A" determines the anterior boundary of the type 3 shadow. The partially rounded edge (Figure 2) has a radius of 0.05 mm or more and causes significant dispersion of rays 3 and 4 so that no shadow forms between red rays 3 and 4. Note: The exact rounding radius of a partially round-edged optic is determined by the manufacturer and is a continuum. As the corner radii become progressively smaller than 0.05 mm, the dispersion of the rays becomes smaller and the type 3 shadow progressively appears with the 2.5 mm pupil.

functional retina. The ora serrata is normally 5.73 ± 0.81 (SD) posterior to Schwalbe line nasally and 6.53 ± 0.75 mm temporally, as shown in our model (Figure 1).^{35,36} Note the SD is ± 0.81 mm nasally, so there is considerable individual variation in the location of the anterior nasal extent of functional retina. For reference, 1.5 mm of distance along the retina corresponds to approximately 5.0 degrees of visual field.³⁷

This second type of shadow, resulting from anterior IOL sharp-edge discontinuity, can only occur if the IOL is located an adequate distance behind the iris to produce a shadow that falls on the functional retina. From our model with the nominal values, the IOL must be approximately 2.3 mm behind the iris for this to occur. This extreme depth of the IOL behind the iris would be very apparent to a clinician at the slitlamp and is far deeper than that reported for negative dysphotopsia (~ 0.4 to 0.5 mm).^{8,9} Therefore, this type 2 shadow is not what has been referred to as negative dysphotopsia over the past 10 years, either.

Type 3 Shadow: Posterior Sharp/Truncated Lens Discontinuity

Figure 4 shows the third type of shadow that occurs in the extreme temporal field (near 90 degrees). The

posterior sharp or truncated edge of the IOL creates a discontinuity at the posterior edge wherein rays passing through the edge of the IOL will be refracted posterior to the rays passing through the posterior surface near the edge. In Figure 12 (left), the ray passing through point "P" creates the posterior boundary of the shadow and the ray passing through point "A" creates the anterior boundary of the shadow. The rounded edge disperses the rays and reduces or eliminates this shadow (Figure 12, right).

The minimum and maximum original ray angle producing type 3 shadows for acrylic and silicone IOLs are shown in the top panels of Figure 13, A and B. The curves and areas between them are very similar with the silicone IOL, producing angles that are slightly smaller than the acrylic IOLs (0.6 degrees to 5 degrees). The upper blue lines are the angles of the original ray from the object forming the posterior border of the Type 3 shadow at various distances of the IOL behind the iris. The lower red lines are the angles of the original ray from the object forming the anterior border of the Type 3 shadow at various distances of the IOL behind the iris. The lower panels (C and D) illustrate the actual retinal field angle (retinal intercept from Table 1) produced by acrylic and silicone. Note the curves are quite different, with the size and extent of the Type 3 shadow (shaded area) being much smaller and more anterior for silicone than acrylic IOLs. The second order regression equations for the upper and lower boundaries of each graph are shown (Figure 13).

The type 3 shadow for an acrylic IOL can be formed 0.06 to 1.23 mm behind the iris, while a silicone IOL would form a shadow 0.06 to 0.62 mm behind the iris. The typical space of 0.45 mm would have a shadow width of approximately 14.0 degrees for acrylic and only approximately 2.3 degrees for silicone, with the posterior border 7.5 degrees more anterior for silicone. This finding is consistent with the clinical observation that negative dysphotopsia is more frequently observed with acrylic IOLs than with silicone IOLs.

Primary optical factors for negative dysphotopsia are a small pupil, a distance behind the pupil of 0.06 mm or larger and 1.20 mm or smaller for acrylic (≥ 0.06 mm and ≤ 0.62 mm for silicone), a sharp-edged design (corner edge radii $\sim \leq 0.05$ mm), a high index of refraction optic, and functional nasal retina that extends anterior to the location of the shadow. Negative dysphotopsia is possible with silicone; however, the probability would be much lower because of the smaller and more anterior location of shadows on the retina as well as the reduced range of distances behind the iris.

The final parameter that determines whether the shadow is visible is the location of the anterior extent of the functional nasal retina. The more anteriorly

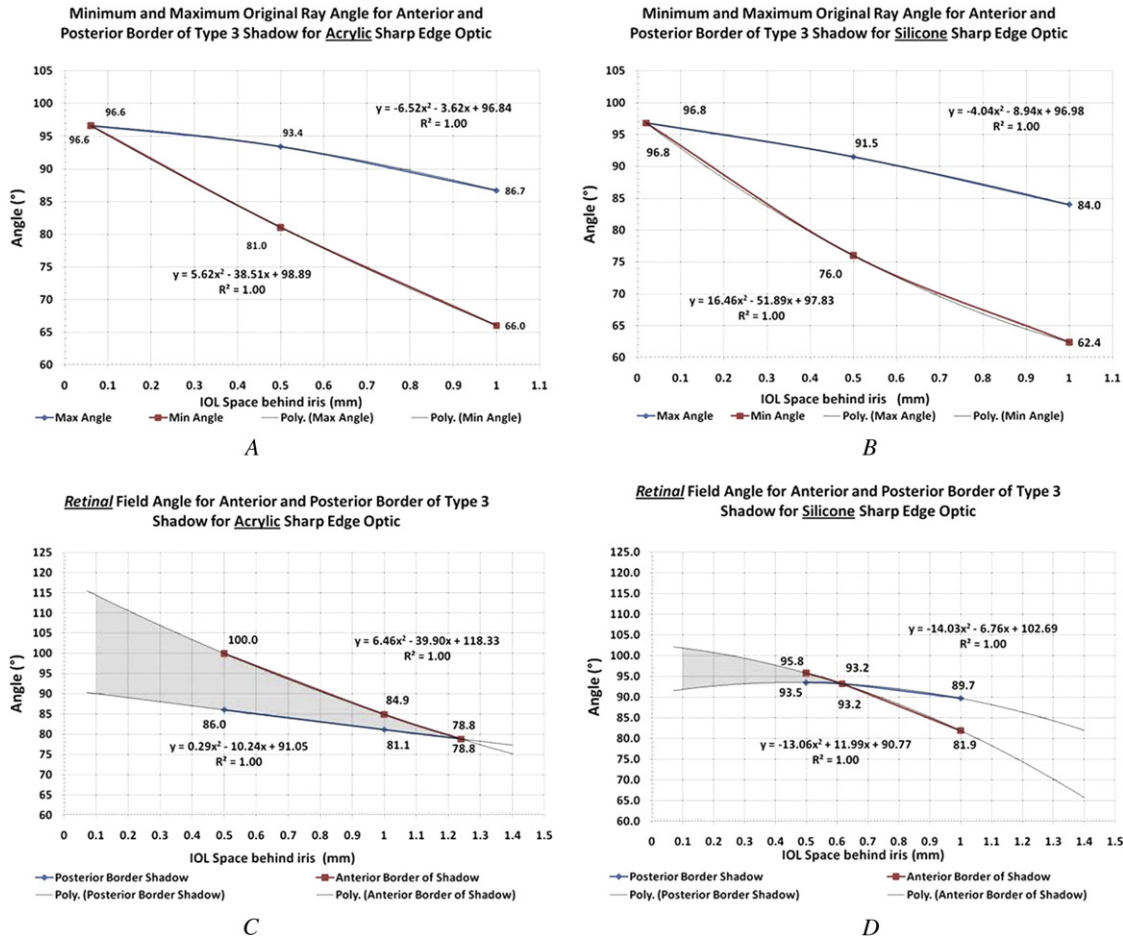


Figure 13. The minimum and maximum original ray angle producing type 3 shadows for acrylic and silicone IOLs are shown on the top row (panels A and B). The curves and areas between them are similar, with the silicone producing angles that are slightly smaller (0.6 to 5.0 degrees). The upper blue lines are the angles of the original ray from the object forming the posterior border of the type 3 shadow at various distances behind the iris. The lower red lines are the angles of the original ray from the object forming the anterior border of the type 3 shadow at various distances behind the iris. The lower row (panels C and D) shows the actual retinal field angle (retinal intercept from Table 1) produced by acrylic and silicone IOLs. Note the curves are quite different, with the size and extent of the type 3 shadow (shaded area) being much smaller for silicone IOLs than for acrylic IOLs. The second-order regression equations for the upper and lower boundaries of each graph are shown (IOL = intraocular lens; Poly. = 2nd-Order polynomial equation).

the functional nasal retina is located, the greater the possibility of seeing the shadow. As mentioned above, the SD for location of the ora serrata relative to Schwalbe line nasally is ± 0.81 mm, a significant variability. In Table 1, for the IOL posterior to the iris by 0.5 mm and the nominal parameters, the anterior border of the 14.0-degree shadow (ray 4 retinal intercept) is $z = 6.254$ mm and $x = -11.825$ mm and the posterior border (ray 3 retinal intercept) is $z = 9.180$ mm and $x = -11.948$ mm. If the “average” anterior border of functional retina were located 0.81 mm (1 SD) posterior to the anterior border of the shadow ($z = 7.064 = 6.254 + 0.81$), 16% of the population would see the complete type 3 shadow immediately after surgery. This location of the functional nasal retina agrees with Moses³⁴ experiments with diascleral visual field mapping mentioned previously and

Osher’s⁸ incidence of negative dysphotopsia of 15.2% on the first postoperative day.

We believe the type 3 shadow is the optical mechanism that has been referred to as negative dysphotopsia by Davison⁴ and explains all 10 clinical manifestations enumerated by Masket and Fram.¹¹

Additional Influences

Secondary factors for negative dysphotopsia are the patient’s angle α and the nasal location of the pupil relative to the optical axis. Angle α is the angle between the visual axis and the optical axis of the eye. The nominal horizontal angle α is approximately 5.2 degrees (0.6 mm on the cornea),³⁸ where the eye is turned temporally, exposing more nasal retina and less temporal retina. Another secondary factor is the decentration of

the pupil, which is displaced nasally, by approximately 2.6 degrees (0.3 mm on the cornea)³⁷ on average, so it is nearer the nasal edge of the IOL than the temporal edge. From Table 1, we see that decentration of the pupil to the normal physiologic position would reduce the retinal field angles to 85.9 degrees and 95.7 degrees, decreasing the width of the retinal field angle of the type 3 shadow for nominal parameters to 9.8 degrees (from 14.0 degrees).

The shadow for the 2.5 mm pupil and nominal parameters is only visible temporally (86.0 degrees to 100.0 degrees) from approximately 55 degrees above and approximately 70 degrees below the horizontal (Figure 8). The extent visible to the patient would depend on the location of the most anterior extent of functional nasal retina. Figure 14 shows actual patient drawings illustrating the extreme temporal location of the shadow. Constriction of the pupil increases the contrast between the shadow and adjacent rays by reducing the cone angle of the pencil of rays from the points in the extreme periphery, similar to the pinhole effect for the foveal image. This was confirmed in our eye model when the 2.5 mm pupil diameter was increased to 5.0 mm and the shadow disappeared due

to the dispersion of rays. If the temporal field is dark (as occurs under scotopic conditions) or the patient uses a cupped hand to shield the temporal visual field, the arcuate shadow would not be visible because of the dark background.⁸

Standard Goldmann and Humphrey visual fields would not show the scotoma because the pupil is large under the low mesopic conditions of the test and most automated visual field analyzers do not extend the 80 degrees to 95 degrees temporal angle necessary to detect negative dysphotopsia. Confrontation fields with a penlight under bright photopic conditions (lights on in the examining room) will show the extreme temporal scotoma when present. It is true that there is a general reduction in threshold sensitivity on visual field testing in pseudophakia, and it is more pronounced in the periphery.³⁹⁻⁴³ However, this generalized reduction in sensitivity could not cause a well-demarcated absolute arcuate scotoma near 90 degrees peripherally and is not localized to nasal retina, as in negative dysphotopsia.

It has also been proposed that the temporal clear corneal incision may be implicated in negative dysphotopsia. Osher⁴⁴ states clearly in his comments on Cooke's

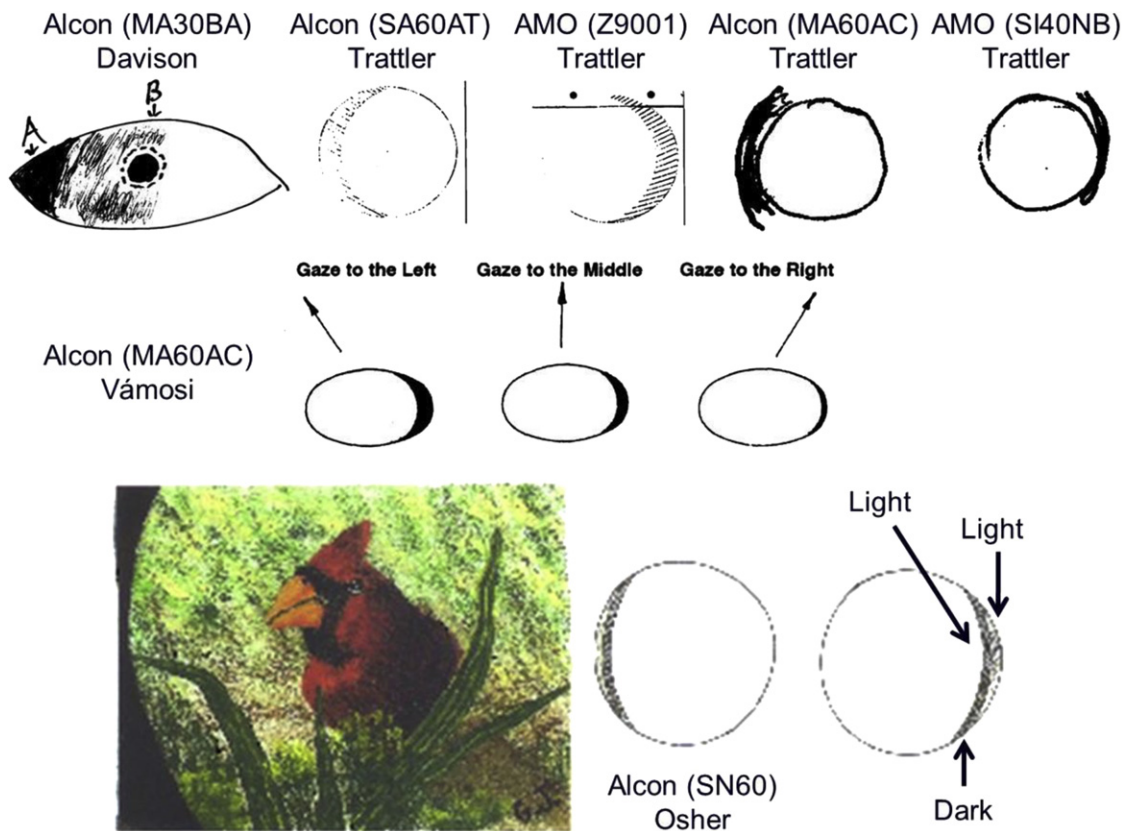


Figure 14. Patient drawings showing the extreme temporal location of the arcuate shadow. Note the light area beyond the shadow in the bottom drawing of patient 4 while only a dark area is indicated in the drawings of the other 3 patients. (Reprinted with permission of the Journal of Cataract & Refractive Surgery.^{4,7-9} Copyright 2000, 2005, 2008, 2010, American Society of Cataract and Refractive Surgery).

article¹³ that “permanent negative dysphotopsia seems related to the contour of the lens optic, primarily its truncated square edge or its edge reflectivity. “Transient” (negative dysphotopsia) symptoms could be due to the broad-based clear or near-clear corneal incisional edema that interferes with oblique light projected into the far peripheral field known as the monocular temporal crescent.” Our article supports Osher’s comments and Cooke’s reply⁴⁵ for “permanent” negative dysphotopsia.

The “transient” shadow on the iris in Figure 2 of Osher’s article⁸ is explained as follows: The illumination beam of the slitlamp is a weakly convergent beam in which the illuminated slit (or round aperture if the slit is wide open) is in focus near the iris plane, which is coincident with the focal plane of the biomicroscope visualization system.³⁷ The optical defect created by the corneal incision causes a shadow because the screen (iris) is so close to the corneal incision. This is analogous to placing one’s finger (opacity or optical defect) on the front of a portion of a projector lens and then placing the screen directly behind the finger—the shadow is well delineated and distinct. As one moves the screen farther from the finger and projector to the normal image distance, the shadow fades and becomes imperceptible. This effect can be seen in Osher’s Figure 2 (B compared with A),⁸ in which the distinct linear shadow becomes a blurred faded crescent when moved just approximately 2.0 mm more centrally on the iris (farther from the incision and cornea). The image becomes curved due to curvature of field.³⁷

By the time rays forming the shadow reach the retina (another 8.0 to 12.0 mm beyond the central iris), the shadow would be indistinct and imperceptible. In short, optical defects in the lens plane (cornea) are not visible at the image plane (retina) but do cause reduction in contrast and image quality from the light

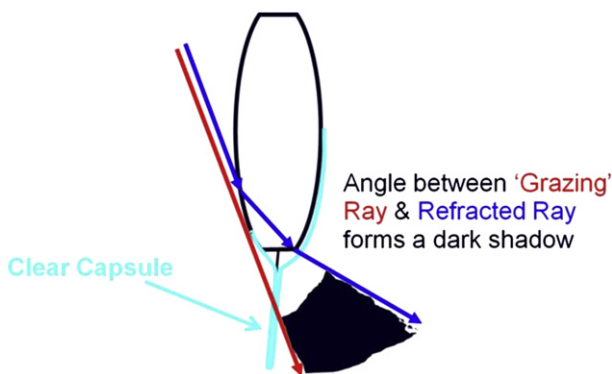


Figure 15. With a round or square-edged optic, the red ray just misses the IOL and is not refracted, while the blue ray strikes the front surface of the IOL and is then refracted by the back surface or the edge of the IOL. The region between the red ray and blue ray would appear as a dark shadow if it falls on functional retina. The clear capsule has no effect on the rays.

scatter. Also, additional clinical studies comparing temporal clear corneal incisions with nasal,⁵ superior,^{6,9} and scleral tunnel⁶ incisions found no difference in the incidence of negative dysphotopsia acutely (transient) or long term (permanent).

Natural Course and Treatments

The spontaneous resolution or transient nature of the negative dysphotopsia can be explained by the opacification (actually translucency) of the nasal capsule in the first few weeks to several months after surgery.⁴⁶⁻⁴⁹ Osher⁸ reported negative dysphotopsia in 15.2% on the first postoperative day, 3.2% at 1 year, and 2.4% at 2 to 3 years. In Figure 15, we see that as long as the nasal capsule remains clear, there is no light scattered into the shadow. However, when the nasal capsule becomes translucent (acts as a diffuser), the scattered rays fill the shadow and eliminate the negative dysphotopsia (Figure 16). Figure 17 shows a clinical example of a nasal capsule that has become translucent using the red reflex.⁴ Only a portion of the nasal peripheral capsule has to become translucent to fill the shadow with scattered rays of light. Posterior capsule opacification (PCO) also causes light scatter, which reduces retinal contrast and results in reduced retinal threshold sensitivity.⁵⁰ Anterior axial movement of the IOL from capsular bag contraction is also a possible explanation for the decreasing incidence over time because it could reduce the axial space behind the iris to 0.06 mm or less. However, it would also be associated with a myopic shift in the patient’s refraction, which is extremely rare with contemporary

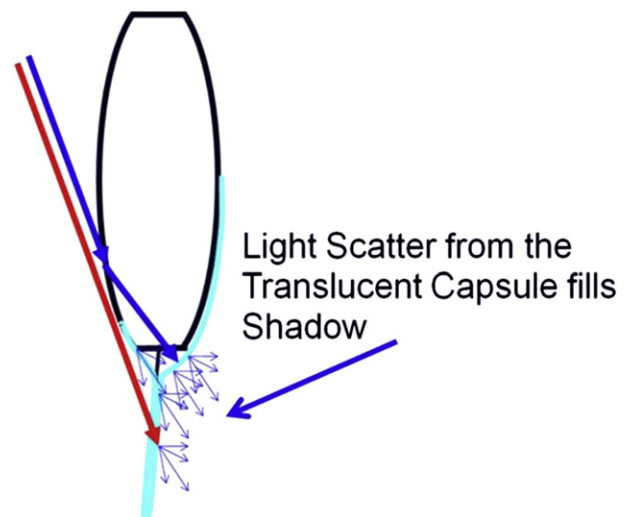


Figure 16. Square-edged optic and light scatter from the capsule. Light scatter from anterior and/or posterior capsule or frosted (textured) edge of an IOL fills either a type 2 or type 3 shadow (Figure 4) with dispersed light making it no longer visible.

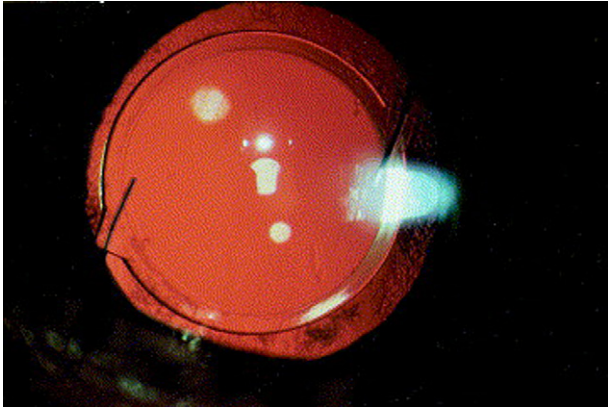


Figure 17. A clinical example of a nasal capsule in a right eye that has become translucent (opacified) using the red reflex. Notice the normal nasal location of the pupil relative to the IOL. (Reprinted with permission of the Journal of Cataract & Refractive Surgery.⁴ Copyright 2000, American Society of Cataract and Refractive Surgery).

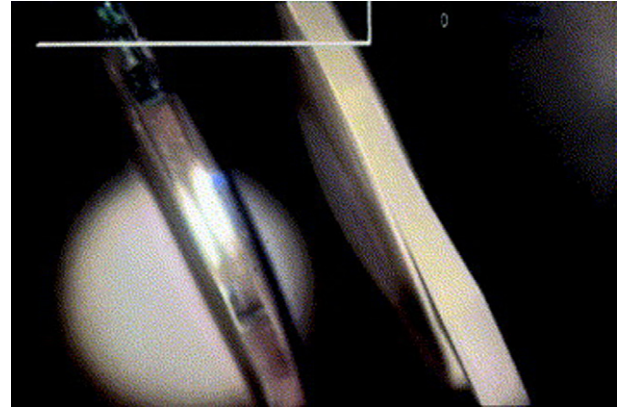


Figure 18. Manufacturers have addressed the problem of negative dysphotopsia by frosting the edge (textured edge) of the IOL (right) compared with an unfrosted (untextured edge) (left). Note how much brighter and distinct the light reflex from the unfrosted edge versus the frosted edge, which scatters the light. (Reprinted with permission of the Journal of Cataract & Refractive Surgery.⁴ Copyright 2000, American Society of Cataract and Refractive Surgery).

IOLs and has not been associated with the disappearance of negative dysphotopsia.

When the nasal capsule remains clear and an explanation of the shadow to the patient does not suffice, surgical intervention may become necessary. Four types of surgical interventions that have been discussed are IOL exchange, piggyback IOLs, reverse optic capture, and iris suture fixation of the capsule bag-IOL complex.

Intraocular lens exchanges have been performed to change (1) sharp-edged acrylic to round-edged silicone, (2) shiny to frosted sharp-edged optics, and (3) reverse-shape optics (posterior surface is flatter than anterior surface). Exchanging sharp-edge acrylic to rounded-edge silicone may not necessarily eliminate the patient's symptoms.⁴ As explained above, silicone moves the type 3 shadow anteriorly and significantly reduces its width; however, it still may be on the functional retina. Although successful in some cases, it only reduces the probability of seeing the shadow. Also, the rounded posterior edge of the IOL has a radius that may be small enough to still perform as a sharp edge. (Sharp- to round-edged optics is a continuum.)

Using a frosted (textured) edge optic for an exchange or as the primary IOL in the second eye lowers the incidence of both positive and negative dysphotopsia (Figure 18).⁴ This type of design roughens (textures) the edge of the IOL optic to create the same type of light scatter as created by translucency of the peripheral, nasal capsule. Frosting also reduces the internal light scatter from a sharp- or truncated-edged optic by dispersing the light that leads to positive dysphotopsia. Using a reverse-shape optic has almost no effect on the position of the shadow so would not be expected to eliminate the negative dysphotopsia.⁴

It has also been observed that in a single-piece posterior chamber IOL, placing the haptics horizontally appears to reduce the incidence of negative dysphotopsia.^A This observation would be supported by the ray-tracing diagram in Figure 4. The edge of the IOL is more peripheral where the shoulder of the haptic inserts into the optic. The exact amount would depend on the design of the haptic. The origin of the rays at the IOL edge would be moved laterally to the edge of the haptic, causing the retinal intercepts of the shadows to be more anterior and smaller in width. These changes would reduce the incidence of negative dysphotopsia, similar to the reduction with silicone versus acrylic optic material described in the section on type 3 shadow and shown in Figure 13, C and D.

A second treatment option for negative dysphotopsia is to place a secondary piggyback IOL in the sulcus.²⁸ This procedure reduces or eliminates the space behind the iris; however, it must be less than 0.06 mm, which is not always the case. A fully round-edged optic reduces the probability that an extreme peripheral ray can strike the edge of the IOL and then fall onto functional retina; however, a second IOL in the sulcus can cause axial movement of the original IOL, resulting in a refractive change. If the primary IOL moves anteriorly, it would increase the effective power, inducing a myopic shift¹⁵; if it moves posteriorly, a hyperopic shift would occur. In either case, an unexpected change in refraction would require a third treatment (usually corneal laser surgery) to adjust the patient's refraction, which is undesirable in an already unhappy patient.

A third treatment option for negative dysphotopsia is reverse optic capture, where the anterior capsule is placed posterior to the IOL optic.¹¹ We agree that this

technique is usually successful in eliminating negative dysphotopsia, but do not agree with Masket and Fram's theory that negative dysphotopsia is from a reflection of the anterior capsulotomy edge projected onto nasal peripheral retina.^{11,51} If this were the case, it would cause a positive dysphotopsia and the reflection would be far too anterior to be on functional retina.

At least 3 of the findings of the hypothesis testing shown in their Table 1 prove that the ray-tracing simulation and explanation of Hong et al.⁵¹ are not negative dysphotopsia. First, the results were "relatively invariant with pupil size and not mitigated when dilated." One hallmark of negative dysphotopsia is that it is worse with pupil constriction and better with the pupil dilated, as we have shown with the 2.5 and 5.0 mm pupils. Second, if negative dysphotopsia were the "dark-arc" or intensity gaps between visible arcs/bands, the dark arc would be reversed (mirrored) with the ends pointing in the opposite direction from the patient drawings in Figure 14. The dark arc would also not be a crescent coming to a point at the end but rather a band that is uniform in width with a flare at the end. Third, the patient experiences negative dysphotopsia in lighted surroundings (lighted examining room or outside, simulated by a Ganzfeld source), not in the dark with a point source at 75 degrees. If Hong et al. were to have used a Ganzfeld source instead of a point source, the dark arcs would disappear because they would be filled by visible arcs/bands from other angles. We do agree with their finding that the spontaneous resolution of negative dysphotopsia is a result of opacification (translucency/diffusivity) of the peripheral capsule, as we have shown in Figure 16.

In addition, when the anterior capsule is moved posterior to the IOL optic, in direct contact with the posterior capsule (reverse optic capture), both surfaces opacify (become translucent), rapidly creating a diffuser that fills the shadow with light (Figure 16). As Hong et al.⁵¹ observed, "a rapid fibrotic posterior capsule opacification [translucency] and capsule contraction occurred." Smith et al.'s study⁵² confirms this outcome (as well as Davison's observations⁴), showing that the anterior capsule overlap on the IOL has a greater effect in reducing PCO than the sharp edge. Sacu et al.⁵³ also found that any attempt to polish the anterior capsule is futile and will have no effect on PCO by 1 year. The opacification of the nasal capsule is the explanation for the efficacy of reverse optic capture, just as in the 12.8% (84% of negative dysphotopsia patients) of cases that spontaneously resolved by 2 to 3 years of the original 15.2% in Osher's study.⁸ However, a 100% PCO rate with reverse optic capture would be unacceptable.

The fourth possible treatment option is iris suture fixation of the capsule bag-IOL complex, which Masket and Fram¹¹ showed was unsuccessful in

eliminating the symptoms of negative dysphotopsia. The explanation of Masket and Fram's¹¹ findings can be seen in Figure 1 of their article. The iris is a very delicate structure, and suturing to the IOL complex moves the iris posteriorly but does not move the IOL anteriorly. This maneuver would have a small effect on the type 3 shadow (negative dysphotopsia) and only the type 2 shadow would be eliminated in that it requires a space behind the iris. If the IOL does not move anteriorly, the shadow will remain at the same location on the retina that it was originally.

Nomenclature

The proper scientific term for a dark crescent-shaped shadow is *penumbra* (Latin, *paene* "almost, nearly, partial" and *umbra* "shadow"). Although most commonly used to describe celestial bodies (partial solar or lunar eclipse), the term *penumbra* is also used in photography, optics, and lighting and is the appropriate term to describe the arcuate shadow seen by patients. The type 3 penumbra (partial shadow) is what has been clinically termed negative dysphotopsia.

In summary, the primary factors determining the presence of negative dysphotopsia are a small pupil, an axial space behind the iris of 0.06 mm or longer and 1.2 mm or shorter for acrylic, and a sharp optic edge (edge radii ≤ 0.05 mm), resulting in a penumbra that falls on the functional retina. Secondary factors include the high index of refraction optic material, specific tilt of the eye (angle α), amount of nasal decentration of the pupil, and transparent versus translucent status of the peripheral nasal capsule. When these primary and secondary factors are present, a penumbra will fall on the inner surface of the eye and if it is functional retina, will result in the phenomenon that has been referred to as negative dysphotopsia.

WHAT WAS KNOWN

- Negative dysphotopsia has been clinically reported using posterior chamber IOLs over the past 12 years with very specific symptoms of a black, temporal crescent in the extreme periphery that is more accentuated by pupil constriction, reduced by pupil dilation, and believed to be related to square-edged optics and higher index of refraction materials; however, no optical ray-tracing studies have validated these observations or proposed explanations.

WHAT THIS PAPER ADDS

- The optical ray tracing using standard techniques shows the cause of negative dysphotopsia and explains some of the perplexing clinical observations that have remained an enigma until now.

ACKNOWLEDGMENTS

The authors would like to acknowledge Guy M. Kezirian and R. Doyle Stulting for their invaluable preparation, review and critique of the manuscript.

REFERENCES

- Holladay JT, Lang A, Portney V. Analysis of edge glare phenomena in intraocular lens edge designs. *J Cataract Refract Surg* 1999; 25:748–752
- Holladay JT, Bishop JE, Lewis JW. Diagnosis and treatment of mysterious light streaks seen by patients following extracapsular cataract extraction. *Am Intra-Ocular Implant Soc J* 1985; 11:21–23
- Holladay JT. Evaluating the intraocular lens optic. *Surv Ophthalmol* 1986; 30:385–390
- Davison JA. Positive and negative dysphotopsia in patients with acrylic intraocular lenses. *J Cataract Refract Surg* 2000; 26:1346–1355
- Narváez J, Banning CS, Stulting RD. Negative dysphotopsia associated with implantation of the Z9000 intraocular lens. *J Cataract Refract Surg* 2005; 31:846–847
- Radford SW, Carlsson AM, Barrett GD. Comparison of pseudophakic dysphotopsia with Akreos Adapt and SN60-AT intraocular lenses. *J Cataract Refract Surg* 2007; 33:88–93
- Trattler WB, Whitsett JC, Simone PA. Negative dysphotopsia after intraocular lens implantation irrespective of design and material. *J Cataract Refract Surg* 2005; 31:841–845
- Osher RH. Negative dysphotopsia: long-term study and possible explanation for transient symptoms. *J Cataract Refract Surg* 2008; 34:1699–1707
- Vámosi P, Csákány B, Németh J. Intraocular lens exchange in patients with negative dysphotopsia symptoms. *J Cataract Refract Surg* 2010; 36:418–424
- Gosala S. Optical phenomena causing negative dysphotopsia [letter]. *J Cataract Refract Surg* 2010; 36:1620; reply by DL Cooke, 1620–1621
- Masket S, Fram NR. Pseudophakic negative dysphotopsia: surgical management and new theory of etiology. *J Cataract Refract Surg* 2011; 37:1199–1207
- Mamalis N. Negative dysphotopsia following cataract surgery [editorial]. *J Cataract Refract Surg* 2010; 36:371–372
- Cooke DL. Negative dysphotopsia after temporal corneal incisions. *J Cataract Refract Surg* 2010; 36:671–672
- Wei M, Brettell D, Bhardwaj G, Francis IC. Negative dysphotopsia with spherical intraocular lenses [letter]. *J Cataract Refract Surg* 2010; 36:1621
- Masket S, Fram NR, Hill WE, Ayers BD, Hamilton DR, Ernest P, Fine IH, Coronea MT, Trattler W. Consultation section: cataract surgical problem. *J Cataract Refract Surg* 2011; 37:421–426
- Erie JC, Bandhauer MH, McLaren JW. Analysis of postoperative glare and intraocular lens design. *J Cataract Refract Surg* 2001; 27:614–621
- Erie JC, Bandhauer MH. Intraocular lens surfaces and their relationship to postoperative glare. *J Cataract Refract Surg* 2003; 29:336–341
- Masket S. Truncated edge design, dysphotopsia, and inhibition of posterior capsule opacification. *J Cataract Refract Surg* 2000; 26:145–147
- Tester R, Pace NL, Samore M, Olson RJ. Dysphotopsia in phakic and pseudophakic patients: incidence and relation to intraocular lens type. *J Cataract Refract Surg* 2000; 26:810–816
- Ellis MF. Sharp-edged intraocular lens design as a cause of permanent glare. *J Cataract Refract Surg* 2001; 27:1061–1064
- Coroneo MT, Pham T, Kwok LS. Off-axis edge glare in pseudophakic dysphotopsia. *J Cataract Refract Surg* 2003; 29:1969–1973
- Franchini A, Zamma Gallarati B, Vaccari E. Computerized analysis of the effects of intraocular lens edge design on the quality of vision in pseudophakic patients. *J Cataract Refract Surg* 2003; 29:342–347
- Wallin TR, Hinckley M, Nilson C, Olson RJ. A clinical comparison of single-piece and three-piece truncated hydrophobic acrylic intraocular lenses. *Am J Ophthalmol* 2003; 136:614–619
- Buehl W, Menapace R, Sacu S, Kriechbaum K, Koeppel C, Wirtitsch M, Georgopoulos M, Findl O. Effect of a silicone intraocular lens with a sharp posterior optic edge on posterior capsule opacification. *J Cataract Refract Surg* 2004; 30:1661–1667
- Hayashi K, Hayashi H. Effect of a modified optic edge design on visual function; textured-edge versus round-anterior, slope-side edge. *J Cataract Refract Surg* 2004; 30:1668–1674
- Buehl W, Findl O, Menapace R, Sacu S, Kriechbaum K, Koeppel C, Wirtitsch M. Long-term effect of optic edge design in an acrylic intraocular lens on posterior capsule opacification. *J Cataract Refract Surg* 2005; 31:954–961
- Shambhu S, Shanmuganathan VA, Charles SJ. The effect of lens design on dysphotopsia in different acrylic IOLs. *Eye* 2005; 19:567–570. Available at: <http://www.nature.com/eye/journal/v19/n5/pdf/6701568a.pdf>. Accessed March 6, 2012
- Ernest PH. Severe photic phenomenon. *J Cataract Refract Surg* 2006; 32:685–686
- Schwiegerling J. Recent developments in pseudophakic dysphotopsia. *Curr Opin Ophthalmol* 2006; 17:27–30
- Shah U. Probable edge defect in Acrysof single-piece intraocular lens. *Indian J Ophthalmol* 2006; 54:277–278. Available at: <http://www.ijo.in/article.asp?issn=0301-4738;year=2006;volume=54;issue=4;spage=277;epage=278;aulast=Shah>. Accessed March 6, 2012
- Wolffe M, Landry RJ, Alpar JJ. Identification of the source of permanent glare from a three-piece IOL. *Eye* 2006; 21:1078–1082. Available at: <http://www.nature.com/eye/journal/v21/n8/pdf/6702539a.pdf>. Accessed March 6, 2012
- Aslam TM, Gupta M, Gilmour D, Patton N, Dhillon B. Long-term prevalence of pseudophakic photic phenomena. *Am J Ophthalmol* 2007; 143:522–524
- Marques FF, Marques DMV. Unilateral dysphotopsia after bilateral intraocular lens implantation using the AR40e IOL model: case report. *Arq Bras Oftalmol* 2007; 70:350–354. Available at: <http://www.scielo.br/pdf/abo/v70n2/29.pdf>. Accessed March 6, 2012
- Moses RA. Accommodation. In: Moses RA, ed, *Adler's Physiology of the Eye; Clinical Application*, 6th ed. St. Louis, MO, Mosby, 1975; 307–308
- Straatsma BR, Foos RY, Spencer LM. The retina: topography and clinical correlations. In: *Symposium on Retina and Retinal Surgery; Transactions of the New Orleans Academy of Ophthalmology*. St. Louis, MO, Mosby, 1969; 1–26
- Straatsma BR, Landers MB, Kreiger AE. The ora serrata in the adult human eye. *Arch Ophthalmol* 1968; 80:3–20
- Michaels DD. *Visual Optics and Refraction; A Clinical Approach*, 3rd ed. St. Louis, MO, Mosby, 1985; 180–181
- Campbell CJ, Koester CJ, Rittler MC, Tackaberry RB. *Physiological Optics*. Hagerstown, MD, Harper & Row, 1974; 97,104–107,178–180
- Flament J, Landre JC, Langer I, Piat JC. Le champ visuel du pseudophake. Étude périmétrique et statistique et statistique [The visual field of pseudophakic patients. Perimetric and statistical study]. *J Fr Ophtalmol* 1987; 10:295–300
- Klewin KM, Radius RL, Schultz RO. Visual-field function in pseudophakia. *Ann Ophthalmol* 1988; 20:316–317

41. Nacef L, Jeddi A, Marrakchi S, Allagui M, Ayed S. Etude du champ visuel du pseudophaque en périmétrie cinétique et automatisée [The visual field of patients with pseudophakia using kinetic and automated perimetry]. *J Fr Ophtalmol* 1992; 15:405–409
42. Omulecki W, Grymin H, Kowalski M. [Visual field in pseudophakia]. [Polish] *Klin Oczna* 1993; 95:384–386
43. Mutlu FM, Akay F, Bayer A. Effect of pseudophakia on standard perimetry parameters. *Curr Eye Res* 2009; 34:711–716
44. Osher RH. Differentiating transient and permanent negative dysphotopsia [letter]. *J Cataract Refract Surg* 2010; 36:1619
45. Cooke DL. Differentiating transient and permanent negative dysphotopsia, reply to RL Osher [letter]. *J Cataract Refract Surg* 2010; 36:1619–1620
46. Birchall W, Brahma AK. Eccentric capsulorhexis and postoperative dysphotopsia following phacoemulsification. *J Cataract Refract Surg* 2004; 30:1378–1381
47. Nadler DJ, Jaffe NS, Clayman HM, Jaffe MS, Luscombe SM. Glare disability in eyes with intraocular lenses. *Am J Ophthalmol* 1984; 97:43–47
48. Kora Y, Marumori M, Kizaki H, Yaguchi S, Kozawa T. Experimental study of small intraocular lenses using an eye model. *J Cataract Refract Surg* 1993; 19:772–775
49. Witmer FK, van den Brom HJB, Kooijman AC, Blanksma LJ. Intra-ocular light scatter in pseudophakia. *Doc Ophthalmol* 1989; 72:335–340
50. García-Medina JJ, García-Medina M, Arbona-Nadal MT, Pinazo-Duran MD. Effect of posterior capsular opacification removal on automated perimetry. *Eye* 2006; 20:537–545. Available at: <http://www.nature.com/eye/journal/v20/n5/pdf/6701918a.pdf>. Accessed March 6, 2012
51. Hong X, Liu Y, Karakelle M, Masket S, Fram NR. Ray-tracing optical modeling of negative dysphotopsia. *J Biomed Opt* 2011; 16:125001
52. Smith SR, Daynes T, Hinckley M, Wallin TR, Olson RJ. The effect of lens edge design versus anterior capsule overlap on posterior capsule opacification. *Am J Ophthalmol* 2004; 138:521–526
53. Sacu S, Menapace R, Findl O, Georgopoulos M, Buehl W, Kriechbaum K, Rainer G. Influence of optic edge design and anterior capsule polishing on posterior capsule fibrosis. *J Cataract Refract Surg* 2004; 30:658–662

OTHER CITED MATERIAL

- A. Stulting RD. Personal communication, November 2011



First author:

Jack T. Holladay, MD, MSEE

*Department of Ophthalmology,
Baylor College of Medicine,
Houston, Texas, USA*